Separation of Colloidal Particles in a Packed Column using Depletion Forces

Francisco J. Guzman

Thesis submitted to the faculty of the Virginia Polytechnic Institute and State University in

partial fulfillment of the requirements for the degree of

Master of Science

In

Chemical Engineering

John Y. Walz

William A. Ducker

Stephen M. Martin

(August 27th 2012)

Blacksburg, VA

Keywords: Colloid Transport, Depletion Forces, Depletion Interaction, Secondary energy well aggregation

Separation of Colloidal Particles in a Packed Column using Depletion Forces

Francisco J. Guzman

ABSTRACT

Depletion forces were used to separate an equinumber density binary dispersion of 1.5 and 0.82 µm polystyrene sulfate (PS) particles. Experiments consisted of injecting a pulse of a binary dispersion of PS particles into the inlet of a packed bed of 0.5 mm silica collector beads. Prior to injection, a carrier fluid of either KCl and KOH electrolyte or a silica nanoparticle dispersion was flowing through the column at steady state. When the carrier fluid was a dispersion of silica nanoparticles, the ratio of PS particles in the column outlet would change from 1:1 big to small particles to slightly over 2:1. This implies that more of the smaller 0.82 µm particles were being trapped on the surface of the collector beads due to depletion forces. Experiments with a single particle type (either 1.5 or 0.82 µm PS particle) were also done and correlated with the binary dispersion measurements. Potential energy profiles between a PS particle and a flat silica plate were calculated. The secondary energy barrier for the 1.5 µm particles was two times greater than for the 0.82 µm particles. Hence, the 0.82 µm particles were more likely to overcome the energy barrier and get trapped on the surface of the collector beads. Although the potential energy profiles were calculated at equilibrium, they can be used as a tool in finding the optimal conditions for separation.

Table of Contents

List of Figures

List of Tables

1. Introduction

Colloidal particle separation techniques can be categorized into two types of separations. The first type is a batch separation where a dispersion of particles is separated in a one closed step[1-3]. A typical example of a batch separation is the centrifugation of a dispersion of particles[3]. As the particles rotate in the centrifuge the denser particles will tend to move to the bottom of the centrifuge tube forming a concentration gradient throughout the tube. Either the supernatant or concentrate at the bottom can be collected and centrifugation repeated. While effective, such a process is rather cumbersome as achieving a thorough separation of a dispersion of particles can involve multiple repetitions.

The second category of particles separation techniques are continuous separations. These processes can be considered as an open system where a dispersion of particles flows from one side of the system to the other. A well-established example of a continuous separation is field-flow fractionation (FFF) first proposed by Giddings in 1966 [4]. In FFF a dispersion of particles flows through a channel where a field is being applied perpendicular to the direction of flow. A common example of FFF is the laminar flow of a dispersion of particles through a channel of membranes in which there is a cross flow (e.g. field) pushing particles into different sections of the parabolic velocity profile. Since different sections have different velocities, particles closer to the walls of the channel will move out of the channel slower. Particles leaving the channel can then be collected and, depending on the instant of collection, the samples will be of a different particle type. Thus the initial dispersion of particles is separated as a function of the behavior of each particle type within the channel. Other type of continuous particle separation techniques include elutriation, filtering through multiple sieves, membrane filtration, and split-flow thin fractionation (SPLITT)[5].

This work proposes a novel continuous particle separation technique that uses depletion forces as the mechanism for separating a dispersion of particles flowing through porous media. This work is based on earlier work by Weronski et al. who, in 2003, showed that negatively charged polystyrene microparticles flowing through a packed bed of negatively charged glass beads could be trapped within the bed by attractive depletion forces arising from negatively-charged silica nanoparticle.[6] In their work a pulse of polystyrene microparticles was injected at the inlet of a packed column of glass beads that had a carrier fluid flowing through it at steady state. The pulse of microparticles moved through the column and flowed into a flow cell which was connected to a UV/Vis spectrophotometer. By analyzing the breakthrough curves, the recovery of the polystyrene particles could be calculated. Weronski et al. showed that when the carrier fluid was a dispersion of nanoparticles the recovery of the polystyrene particles was as low as 34%, whereas non-nanoparticle experiments had recoveries near 100%. When the carrier fluid was switched from a dispersion of nanoparticles to either an electrolyte or water, some of the trapped particles were released. This implied that the trapped particles were trapped in secondary energy wells that were removed once the carrier fluid was changed. The authors concluded that the particle recovery was a decreasing function of the silica nanoparticle concentration and the carrier fluid residence time, and an increasing function of the velocity in the bed.

My goal in this thesis was to extend this idea to a binary dispersion of particle to specifically test whether depletion forces could lead to particle separations.

Although some groups have used depletion forces to separate particles, non-have developed a continuous method or technique for particle separation. J. Bibette used depletion interactions to purify a polydisperse emulsion via a batch fractionating crystallization scheme[1]. In this work, a silicone oil-water emulsion was purified using sodium dodecyl sulfate (SDS). SDS was added to the oil-water emulsion to a concentration of 0.02 M, just above the critical micelle concentration (cmc). After 24

hours, the top layer would cream and would be separated into a different container. SDS at a slightly higher concentration would be added again to the two different mixtures and the process repeated until a narrow droplet size distribution was reached.

Park et al. separated a dispersion of gold nanorods and nanospheres using a micelle induced depletion interaction[2]. When cetyltrimethyl ammonium bromide (CTAB) surfactant was added to the dispersion, the gold nanorods would aggregate and sediment to the bottom of the container leaving the nanospheres in the supernatant. After only one sedimentation step, the number fraction of rods could be increased from 77% to ~ 99%.

Khripin et al separated a mixture of different length carbon nanotubes by adding polyethylene glycol (PEG) in stepwise increases [3]. As the mixture would precipitate, either the supernatant or sediment would be removed and the addition of PEG repeated.

As suggested by these earlier works, depletion-induced separation of particles is a viable technique that could be applied to a wide range of systems. What all of these technique have in common is that they are batch processes that usually involve multiple steps to achieve the desired separation. One major advantage of the presented work is that rather than having multiple separation steps, the extent of separation can be controlled by changing the residence time of the particle dispersion within the packed bed. This change can be easily done in multiple ways, such as changing the flow rate of the carrier fluid or changing the length of the packed bed. Other applications include studying the effects of the depletion interaction of irregular shaped particles in porous media, a problem that is analogous to the transport groundwater contaminants in natural aquifers.

1.2 Depletion Interaction

The depletion interaction was first successfully explained by Asakura and Oosawa (AO) as an attractive force acting between two colloidal particles of radius r_p suspended in a dilute monodisperse solution of smaller polymer macromolecules of radius r_m [7-8]. The model assumes that all of the particles and macromolecules in the system are behaving as hard spheres (e.g. uncharged) and the macromolecules did not adsorb. When the distance between two colloidal particles is less than diameter of the macromolecules ($2r_m$), the macromolecules are excluded from the region between the particles, resulting in a region of pure solvent between the two particles. As a result there is an osmotic pressure difference between the inner region and the bulk where the macromolecules are located. This pressure difference creates a force acting on the outside of the particles (equivalent to the osmotic pressure of the solution of macromolecules) bringing the particles inward.

An alternative way of explaining the depletion interaction is the loss of free volume available to the macromolecules due to the presence of the larger particles[9]. Around each of the particles there is a region of volume (i.e. a depletion zone) at a distance r_m from the surface such that the center of the macromolecules cannot get closer. As two particles approach each other the depletion zones overlap, thus increasing the volume available to the macromolecules, and hence, increasing conformational entropy of the macromolecules. This leads to a decrease of the free energy of the system since the overall entropy of the system is increasing.

Note that the Asakura-Oosawa potential predicts that the depletion interaction is always attractive. However, various groups have shown experimentally that the depletion interaction can be either attractive (depletion flocculation) or repulsive (depletion stabilization). Feign and Napper first postulated the concept of depletion stabilization using the free energies of mixing [10-11]. Again, consider two uncharged colloidal particles of radius r_p suspended in solution of uncharged non-absorbing

monodisperse spherical macromolecules of radius r_m. As the two colloidal particles approach each other as a function of distance, D, three domains can be considered. In the first domain ($D \geq 4r_m$) the colloidal particles are far enough apart that as they approach each other there is no net free energy change associated with bringing the particles together. There is no net free energy change because the concentration of the macromolecules between the colloidal particles is the same as that of the bulk (the final and initial mixing states are the same). In the second domain ($2r_m \leq D < 4r_m$) as the colloidal particles are approaching each other the macromolecules within the gap region are less evenly distributed and have a lower entropy than that of the bulk. As a result the free energy increases, and hence there is a repulsive interaction between the colloidal particles. The repulsive interaction increases with increasing macromolecule concentration, and at a high enough concentrations flocculation can be prevented. In the third region ($D < 2r_m$) there are no macromolecules and the free energy approaches a minimum as the colloidal particles approach each other.

In aqueous system particles will particles normally acquire a charge, and at high enough macromolecule concentrations, 2nd order effects (macromolecule-macromolecule interactions) need to be considered. Using a force balance on colloidal particles in a solution of monodisperse non-absorbing macromolecules, Walz and Sharma accounted for the effects of charge and higher concentrations of macromolecules and compared their results to the AO model[12]. Details of the model can be seen in section 2.2 of this thesis. At a constant surface potential (-50mV for both particles and macromolecules) increasing the Debye length increases the magnitude and range of the depletion interactions. At a fixed Debye length (10 nm) increasing the magnitude of the surface potential increases the range and magnitude of the depletion attraction. When the interactions among the macromolecules are considered, a long-range repulsion develops followed by a depletion attraction a smaller separation distances. At low macromolecule concentrations (e.g., < 0.5% v) the repulsive depletion barrier is not enough to prevent flocculation while at higher macromolecules concentrations (e.g., >1% v) stability can

be enhanced (e.g. depletion stabilization). Furthermore the authors also showed that the depletion repulsion and depletion attraction increases roughly linearly with particle size.

1.2 Outline of Thesis

The remainder of this thesis is divided into 8 chapters. Chapter 2 focuses on particle transport in packed beds and the theory behind the potential energy profiles between a colloidal particle and a flat plate with a strong emphasis on the depletion force model by Walz and Sharma. Chapter 3 and 4 describe the material and methods section and results. Chapter 5 is the discussion section and is divided into two parts. The first part provides a summary of the results highlighting the key observations. The second section explains the observed results and correlates them to the potential energy profiles calculated using the model described in chapter 2.2. Chapter 6, 7, and 8 are organized as the conclusion, future work, and references sections.

2. Theory

2.1 Particle Transport in Packed Beds

There are several geometrical models simplifying the structure within porous media. Among them are the capillary tube, the constricted tube, and a sphere-in-shell[13-14]. Of these models, the capillary tube is one of the oldest and most straightforward to understand. This model proposes that a packed bed can be represented as a series of capillary tubes arranged in parallel where the flow field inside the capillary is Poiseuillian (see Fig 1).

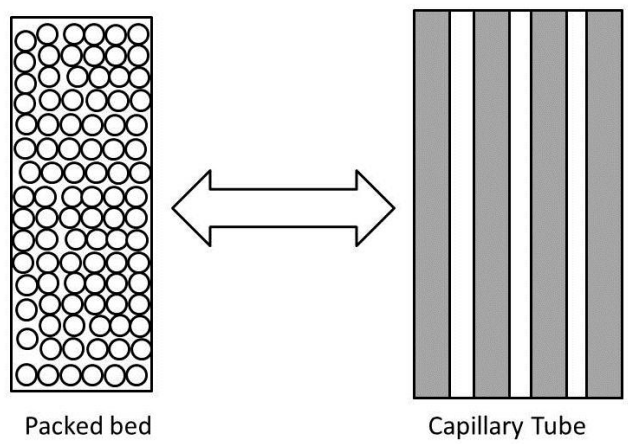

Figure 1: Schematic representation of porous media using the capillary tube model.

Using this model, it is understood that any adsorbed particles are being trapped at the walls of the capillary tube. However, since $R_{Collector} > 325*R_{Particles}$, in our experiments, it is safe to assume that when a particle approaches the surface of a collector bead the interaction can be considered as that of a sphere-plane or sphere-wall.

The radius of the capillary is given by

$$r_{cap} = \sqrt{\frac{8k}{\varepsilon}} \tag{2.1.1}$$

and the flow field within the capillary is

$$u_{cap} = \frac{2u_s}{\varepsilon}[1 - (\frac{r}{r_{cap}})^2] \quad (2.1.2)$$

where ε is the porosity, u_s is the superficial velocity in an empty column, and k is the permeability given by the Carman-Kozeny equation [13]

$$k = \frac{\varepsilon^3 <2R_{collector}>}{180(1-\varepsilon)^2} \quad (2.1.3)$$

The average velocity of the fluid within the capillary can then be calculated as

$$< u_{cap} >= \frac{\int_0^{2\pi}\int_0^R u_{cap} r dr d\theta}{\int_0^{2\pi}\int_0^R r dr d\theta} \quad (2.1.4)$$

where R is the radius of the capillary.

As mentioned in Materials and Method, it is assumed that the collector beads in our system are arranged as a random close packed structure with a porosity of 0.36 [15].

Another pair of useful tools in describing the transport properties are the Reynolds and Peclet number. The Reynolds number is defined as

$$Re = \frac{l_0 v \rho}{\mu} \quad (2.1.5)$$

where l_0 is the characteristic length (diameter of an empty column or the diameter of the capillary), v is the velocity of the fluid, is the density of the fluid, and μ is the viscosity of the fluid. The Reynolds number provides a ratio of the inertial to viscous forces[16] . At low Reynolds' numbers the inertial force can be neglected. For flow in a packed bed the interstitial velocity within the pores can be calculated as

$$v_{inter} = \frac{v_{super}}{\epsilon} \quad (2.1.6)$$

where v_{super} is the superficial or average velocity in an empty column and ε is the porosity of the bed [17].

The Peclet number is defined as

$$Pe = \frac{l_0 v}{D} \tag{2.1.7}$$

where l_0 is the characteristic length, v is the velocity of the fluid, and D is the diffusion coefficient. The Peclet number gives the ratio of the advection of a particle to its diffusion within a given flow field [16]. At high Peclet numbers a particle's movement is predominately due to the bulk fluid and not diffusion. The diffusion coefficient for a spherical particle, D, is calculated using the Stokes-Einstein equation

$$D = \frac{k_B T}{6\pi\mu R_{particle}} \tag{2.1.8}$$

where k_B is the Boltzmann constant, T the temperature of the fluid, μ is the viscosity of the fluid, and $R_{particle}$ the radius of the particles [18].

2.2 Potential Energy Profiles

The depletion interaction potential between a particle in solution and a collector plate were calculated using the depletion force developed by Walz and Sharma [12]. The model calculates the depletion force between two charged spheres in a solution of charged nanoparticles. Using a force balance, the total vector force exerted on particle 1 by the surrounding nanoparticles can be calculated as

$$\boldsymbol{F_1} = \iiint_{\boldsymbol{V}} \rho(\boldsymbol{x}_1)\nabla_1 E(\boldsymbol{x}_1) d\boldsymbol{x}_1 \tag{2.2.1}$$

where $\rho(\mathbf{x_1})$ is the number density of the nanoparticles at position $\mathbf{x_1}$, and $\nabla_1 E(\boldsymbol{x}_1)$ is the gradient of the interaction potential with respect to particle 1 (see Fig. 2) [12].

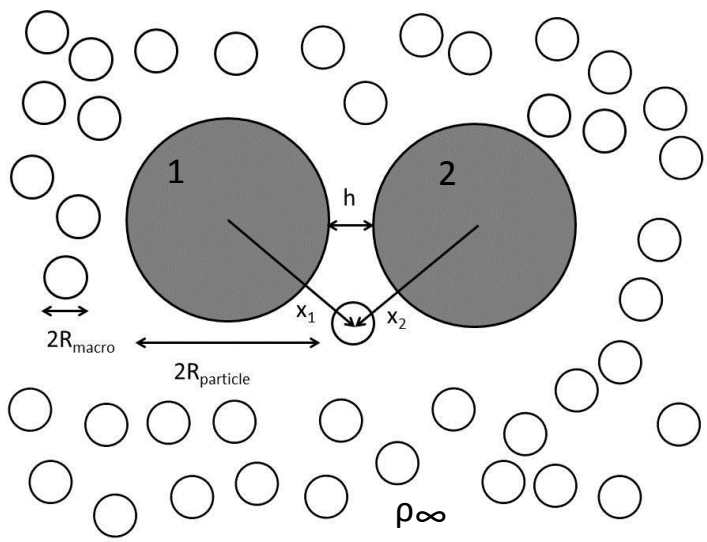

Figure 2: Schematic defining variables used in depletion force equation. [12] R_{macro} is the radius of the macromolecules, $R_{particle}$ the radius of the particles, h is the gap distance, and ρ_∞ is the bulk nanoparticle number density. $\mathbf{X_1}$ and $\mathbf{X_2}$ are vectors defining the position of a nanoparticle relative to the center of a particle 1 and 2 with radius $R_{particle}$.

Since there are two particles 1 and 2 present, E(**x**) can be represented as the sum of two potentials acting on a macromolecule as

$$E(\boldsymbol{x}) = E(\boldsymbol{x_1}) + E(\boldsymbol{x_2}) \tag{2.2.2}$$

where E($\mathbf{x_1}$) is the potential acting on a nanoparticle by particle 1 and E($\mathbf{x_2}$) is the potential acting on a nanoparticle by particle 2. The potential E(**x**) can be further described as the sum of a van der Waals energy, E_{VDW}, and an electrostatic repulsion, $E_{electric}$. E_{VDW} is calculated using the expression for the unretarded van der Waals potential energy for a sphere-sphere geometry and $E_{electric}$ using the linear superposition approximation developed by Bell et al [19-20].

The nanoparticle number density is expressed using a 2nd order virial expansion in bulk nanoparticle number density, which can be written as

$$\rho(\boldsymbol{x}) = \rho_\infty e^{\frac{-E(x)}{k_B T}}[1 + b_1(\boldsymbol{x})\rho_\infty + b_2(\boldsymbol{x})\rho_\infty{}^2 + O(\rho_\infty{}^3)] \tag{2.2.3}$$

where E(**x**) is the potential energy of a nanoparticle at position **x**, b1 is the virial coefficient accounting for interaction between the two nanoparticles, b2 is the interaction between 3 nanoparticles, and so on [12]. This expansion of ρ(**x**) gives rise to a depletion repulsion that is otherwise not seen in the Asakura and Oosawa model. Because of the complexity in mathematically describing the virial coefficients, $\rho(\boldsymbol{x})$ is truncated after the second term (b1) [12]. Considering that there are two particles ρ(**x**) in the presence of nanoparticles, the density expansion is

$$\rho(\boldsymbol{x}) = \rho_\infty e^{\frac{-[E(\boldsymbol{x}1)+E(\boldsymbol{x}2)]}{k_B T}}[1 + b_1(\boldsymbol{x_1})\rho_\infty + b_1(\boldsymbol{x_2})\rho_\infty] \tag{2.2.4}$$

which assumes that the virial coefficients are additive [12]. The final result for the depletion force acting on 1 particle is

$$\boldsymbol{F_1} = \iiint_V \rho_\infty e^{\frac{-[E(\boldsymbol{x_1})+E(\boldsymbol{x_2})]}{k_B T}}[1 + b_1(\boldsymbol{x_1})\rho_\infty + b1(\boldsymbol{x_2})\rho_\infty]\,\nabla_1 E(\boldsymbol{x}_1)d\boldsymbol{x}_1 \tag{2.2.5}$$

which is the equation used in all of the model calculations. The above equation can be integrated as a function of separation distance h to obtain the energy profile. The Derjaguin approximation is then used to estimate the interactions between a particle and a plate[21] .

3. Materials and Methods

3.1 Colloidal Particles and Porous Media

Sulfonates-polystyrene (PS) micro particles were purchased from Spherotech (Lake Forest, IL) (0.82 µm +/- 0.0185 µm) and Invitrogen (Grand Island, NY) (1.5 µm +/1 0.026 µm). SM-30 colloidal silica (11-12 nm) was bought from Fisher Scientific (Waltham, MA) and used as the nanoparticles. Stock SM-30 was cleaned by diluting to a concentration of 9.0% v, adding ion exchange resin to the dilute dispersion, and placed in a rotator for 24 hours. The ion exchange resin was then removed and the nanoparticle dispersion further diluted to a concentration of 3.0% v.

Silica grinding beads (0.5 mm) purchased from OPS Diagnostics (Lebanon, NJ) were used as the granular porous medium. Before each set of experiments the silica beads were put placed in a rotator for 15 min in 10 % w/v NaOH. The beads were then rinsed with ethanol and deionized water followed by a final rinse with deionized water only. The beads were not dried and remained wet the entire time. The day of the experiment the beads were poured into the column and the column was gently vibrated ensuring a close random packed structure. When a bed of glass beads is shaken or vibrated it can reach a minimum porosity of 0.36 [15].

3.2 Column Setup

Colloid transport experiments were conducted by injecting a small volume pulse of PS particles – suspended in a solution of equal pH, ionic concentration, and nanoparticle volume fraction to that of the carrier fluid used in the transport experiment – into the inlet of the column. Prior to injection the carrier fluid was already flowing through the column at steady state. In the depletion experiments the carrier fluid was a 3.0 % v silica nanoparticle solution. The measured pH ranged from 9.23 – 10.44 and the conductivity from 0.99 – 1.1 mS/cm. Control experiments were done with an electrolyte consisting of

KCl, KOH and no silica nanoparticles. The measured pH and conductivity ranged from 9.5 -10.47 and 0.98 – 1.3 mS/cm, respectively, similar to that of the depletion experiments.

The column itself was a 500 x 10 mm borosilicate liquid chromatography column purchased from Omnifit (Danbury, CT). It had two adjustable bed pieces allowing the length of the packed bed to range anywhere from 200 to 500 mm. The end pieces were modified by attaching a single layer of a 120 µm Nitex nylon mesh. The mesh was used to prevent the packing from moving into the bore of the end pieces. The tubing used was a 0.7 mm inner diameter and 1.6 mm outer diameter Teflon tubing purchased from Agilent. For these experiments the bed length was 375 mm with an extra 5 mm as overhead room. The column was wet-packed to minimize air bubbles within the column. Once the column was packed, both the control and depletion experiments were done on the same day and in that order.

As seen in the schematic (Figure 3) the particles are pumped through the column into a flow cell where absorbance measurements are being continually taken. The mass of particles injected into the column was calculated by using the initial concentration of the particle mixture, the flow rate, and the duration of the pulse.

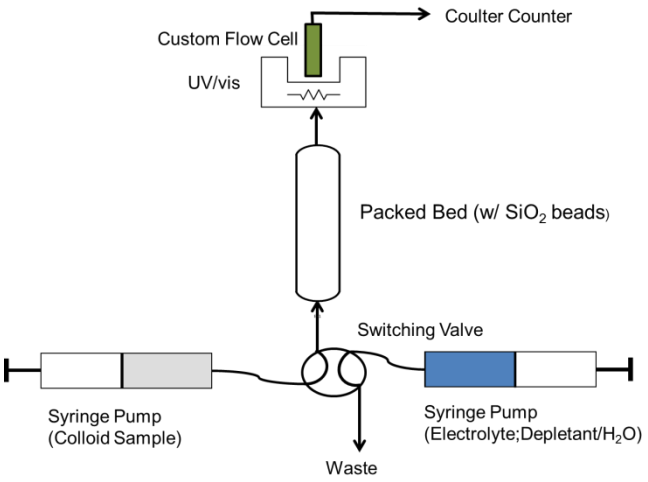

Figure 3: Schematic of the Column setup.

For all of the experiments the pulse length was 8 minutes and the flow rate was 0.30 mL/min. Once the 8 min mark was reached, the carrier fluid was switched from the colloidal sample to the respective carrier fluid of that experiment (e.g. electrolyte for the control experiments, 3.0% SiO_2 for the depletion experiments). The carrier fluid continued to flow through the column and then passed through the flow cell and UV/vis. Here the samples were collected and the concentration of particles determined using a Coulter counter.

Fluid flow through the column and flow cell was always bottom-up. This was done to minimize the effects of sedimentation, ensuring that the depletion attraction was the dominant mechanism for separation. This also helped in the removal of bubbles, as any bubbles formed would move in the direction flow. Before experiments, deionized water was pumped through the column at a flow rate much greater than that of the experiments (> 2 mL/min). Once a blank was measured, an electrolyte (KCL and KOH in water) was pumped through the column, also at a high flow rate. The absorbance was then measured until the measurement stopped changing with time. This was done to ensure that the concentration of electrolyte inside the column was at steady state. Before starting the control or depletion experiment, the flow rate was lowered to 0.30 mL/min and another absorbance measurement taken showing that there was no absorbance dependence on velocity.

In between the control and depletion experiments, water was also pumped at a high flow rate until the absorbance spectra was similar to that of deionized water. The column itself was not taken apart and repacked, however based on the measured absorbance spectra it is safe to assume that absorbance effects of any leftover particles and electrolyte was negligible. By not disassembling the column, the packing length and porosity remain the same. Since the column itself was wet packed, the porosity itself could not be measured accurately, thus the packing density was taken to be 0.64 (or porosity of 0.36), which is a typical value for a random close packed structure [15].

It is noteworthy to mention that although important, the porosity is actually not a crucial factor for the success of this project. As long as it does not change significantly in between sets of experiments, the residence time for the particles within the column should, on average, remain similar. Furthermore, no crucial calculations depend on the porosity. Rather, it is a useful parameter in determining when the particles will leave the column and hence when the effluent collection should start. The porosity can also be used to get an estimate of the residence time of the particles within the column. The residence time is used as tool in double checking that the flow rate is consistent in between sets of experiments.

3.3 Custom Flow Cell

All of the absorbance measurements of the particles in the UV/Vis were done in a custom built flow cell (see Fig. 4). The flow cell is a 12.5 x 12.5 x 50 mm Teflon block with a 3 mm inner diameter and 1.5 mm outer diameter piece of quartz tubing inserted at 1 mm from the front and 6.25 mm from the side of the teflon block (see Figure 2 below). At 15 mm from the bottom and 6.25 mm from the side of the Teflon block, there is a 1 mm bore that is perpendicular to the quartz tubing to allow light to pass. At both the bottom and the top of the flow cell there is a #60 O-ring and Vici Valco (Houston, TX) flangeless PEEK tube end fitting. The fitting has a collapsible ferrule with a 1.5 mm inner diameter.

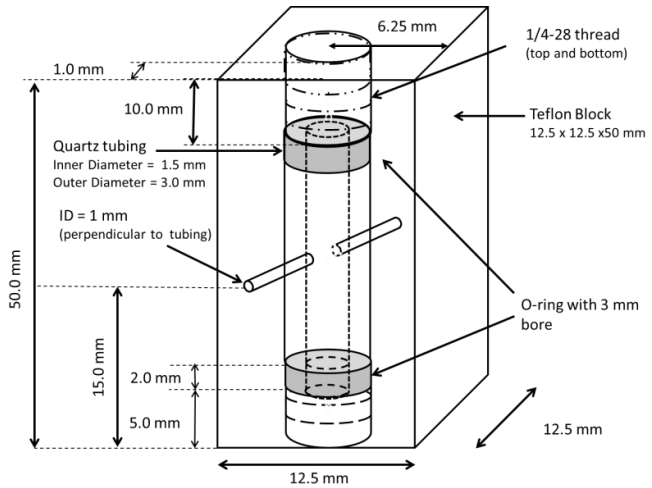

Figure 4: Schematic of custom built flow cell.

One crucial feature of this custom flow cell is that the inner diameters of the quartz tubing, the fitting, and the tubing are very close together. This minimizes the effects of the particles mixing due to diffusion within the flow cell [6]. Unwanted mixing can cause local concentration gradients to develop inside the cell, which could result in absorbance measurements that were not truly representative. By having a flow cell where the change in size from the tubing to into the flow cell is minimal, the effects of such mixing would be small..

However, one caveat of this custom flow cell is that the signal to noise ratio of the measure absorbance spectra increases. In order to overcome this problem two steps are taken[6]. First, the integration time was increased from 0.5 s to 1.8 s. Second, the intensity is averaged over a 100 nm (350 – 450 nm) wavelength range. This means that every absorbance spectra measured is collected over 1.8s and the absorbance data per curve used to plot the breakthrough curves as a function of time is an average over 100 data points.

Once the experiment is assembled, samples are collected continuously for 400 seconds in 400 second intervals starting at the moment the pulse is injected. This fractionates the experiment into multiple regions with different particle concentrations at different times or pore volumes of the experiment. A sample was also collected prior to injection of the pulse and used as a control concentration for each experiment. Collected samples were then mixed well and diluted for analysis in the Coulter Counter.

3.4 Characterization, Instrumentation, and Techniques

The predominant instruments used are an Agilent 8453 UV-Visible Spectrophotometer with the advanced software package (G1116AA) and a Multisizer 4 Beckman Coulter Counter. Other instruments used include a Zen 3600 Malvern Zetasizer, and a pH and conductivity probe.

The 8453 UV/Vis is a single beam spectrophotometer using a deuterium and tungsten lamp. Because it is a single beam spectrophotometer, a reference intensity spectrum must be measured. For all of the measurements taken, the reference blank spectrum was deionized water. In between sets of experiments (e.g. control and then depletion) a new blank reference spectrum was taken. For single particle studies the UV/Vis was calibrated on the day of the experiment using 4, 10, and 30 fold dilutions of the 2.47 x 10^8 #particle/mL initial particle number density used. The calibration follows the linear Beer-Lambert law with zero offset. The 1/slope of the calibration curve constant was used to convert absorbance into concentration.

The calibration measurements were done in the flow cell but without having the particles flow through the column. A typical calibration curve can be seen in Figure 5. In this case the calibration is for a 0.82 µm dispersion with concentrations of 7.49 *10^{-6}, 1.75 *10^{-6}, 7.50 *10^{-6}, 2.5 *10^{-6} g/mL. The zero point is the absorbance for deionized water without any particles.

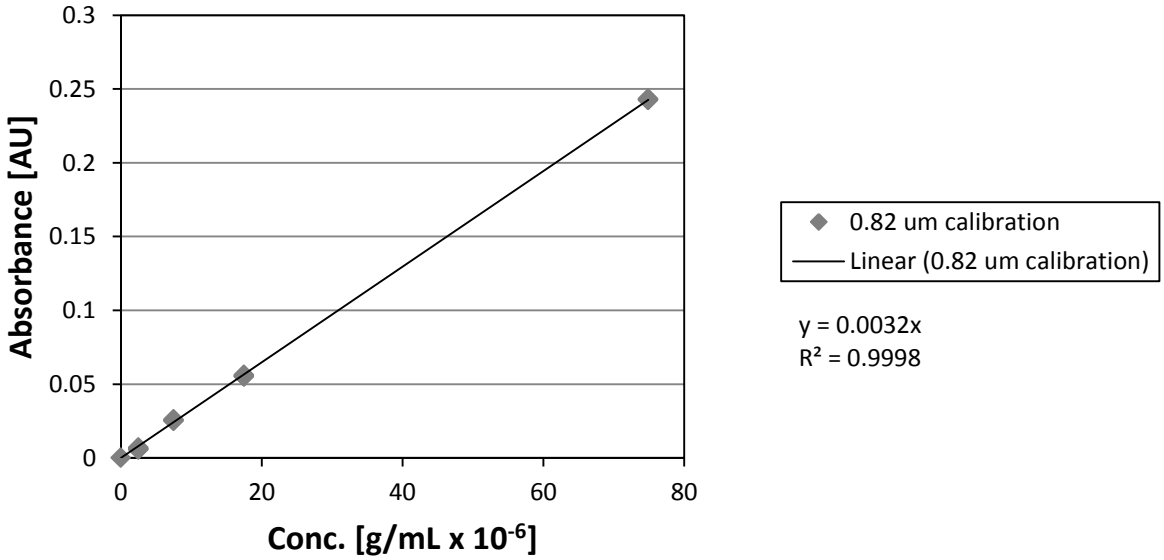

Figure 5: Calibration curve for a 0.82 µm particle dispersion.

The Multisizer 4 (MS4) Beckman Coulter Counter was used to determine the particle concentrations of the collected samples. In the MS 4 particles are suspended in a weak electrolyte solution and drawn through a small aperture tube where voltage is applied across aperture. As a particle passes through the aperture there is a change in the voltage proportional to the particles volume. The instrument then calculates a particle size assuming that the particles are spherical in shape. The aperture tube was calibrated when it was installed and only needs to be calibrated once. However, the calibration was always verified once per working day using 201 fold dilution of 2.022 µm NIST traceable standards. The collected samples were also diluted 201 times before being analyzed inn the coulter counter. A 201 dilution factor was setup into the properties of the measurement. As a result the concentration measurements given by the MS4 were that of the actual sample collected.

3.5 Salt concentration and pH

SM-30 silica nanoparticles, which had been cleaned by ion exchange, were diluted to a 3.0% v concentration. The pH and conductivity was measured as is without any excess KCl or KOH being added. The resulting conductivity values were between 0.99 to 1.0 mS/cm and the pH between 10.28 – 10.44.

It is straightforward to first make a 3.0% by volume nanoparticle solution and then titrate KCl and KOH aliquots into deionized water in order for the carrier fluid of the control experiments to have the same pH and ionic strength as that of the depletion experiments. Although the conductivities of the depletion and control experiments are similar, the exact distribution of the counter ions in the nanoparticle solutions is unknown. According to manufacturer specifications, the nanoparticles contain 0.03% by w/v Na_2SO_4. Conductivity standards were compared to those by Hamer and Kay and are in good agreement [22].

4. Results

4.1. Single particle breakthrough curves

Single particle studies were done using either a 0.82µm or 1.5µm diameter polystyrene particles at a number density of 2.47 * 10^8 particles/mL. The UV/VIS was calibrated, as described in the Materials and Methods section, before each experiment using the appropriate particle size.

The recovery of particles at the column outlet was calculated as

$$\eta = 100\% m_i / m_0 \tag{4.1.1}$$

where

$$m_i = Q \int_0^{t_f} c(t) dt \tag{4.2.2}$$

is the total mass of polystyrene particles detected from the start of the experiment until time t_f. Here c(t) is the time dependent concentration, m_0 is the total mass of particles injected, and Q is the volumetric flow rate [6]. The percentage of particles that remain in the column can then be calculated as 100 – η. For the experiments with nanoparticles the curves had to be shifted to zero because the nanoparticles increased the baseline intensity (compared to water or electrolyte). As seen in Figure 6, there is a significant offset between the measured and modified breakthrough curves for a depletion experiment. This effect arises from an effective increase in absorbance due to the nanoparticles themselves. Because of this the concentration (or absorbance) at 1000 seconds was subtracted from every point in the curve. Every single depletion curve shown henceforth used the same procedure.

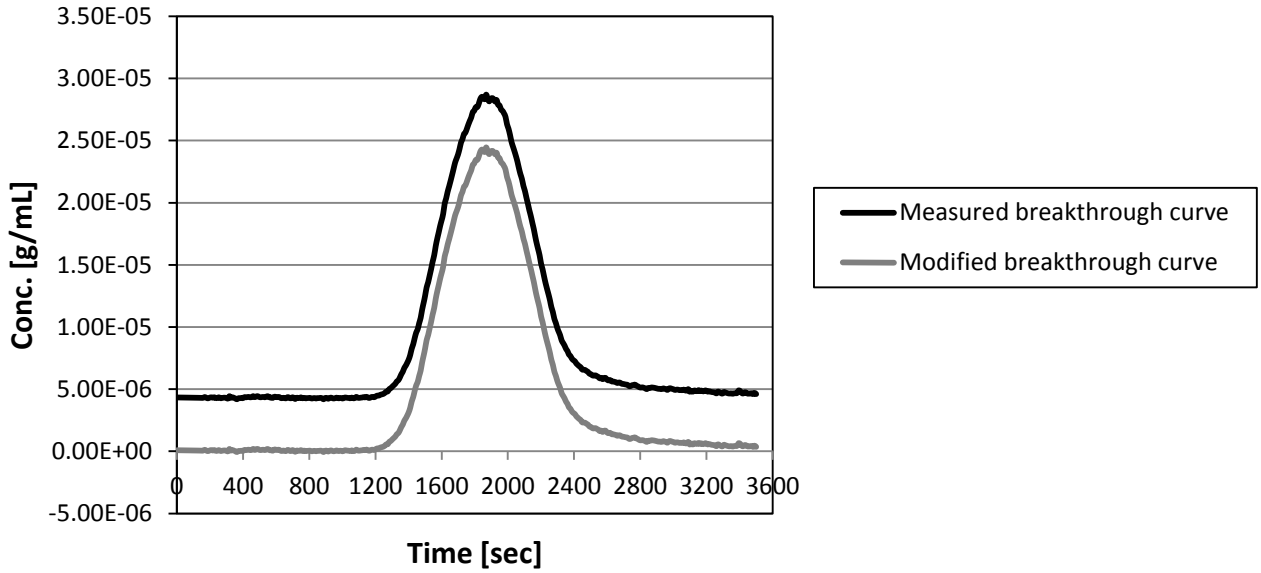

Figure 6: Comparison of measured breakthrough curve data (black line) with the modified (shifted) breakthrough curve (gray line) for a depletion experiment.

In Figure 7A (0.82 µm dispersion), the calculated recoveries are 90% and 45% for the control, e.g. no nanoparticles, and depletion experiments respectively, respectively showing that the depletion attraction has a significant role in capturing the particles within the packed bed. Comparing the control and depletion experiments, the breakthrough curve for the depletion experiments has a long tail after about 2400 seconds. This tail implies that while the particles are trapped within the packed bed some of them are able to escape. (An alternate explanation would be that some of the particles transport through the bed at a slower rate.)

In Figure 7B (1.5 µm dispersion) the calculated recoveries are 103% and 75% for the control and depletion experiments respectively. In this case both the control and depletion breakthrough curves show a significant tailing after about 2400 seconds. Comparing the recoveries of the 0.82 µm and 1.5 µm depletion experiments, it is shown that more of the smaller particles are captured within the packed bed. However, in all cases there is a significant decrease in the recovery, η, of the polystyrene particles compared to the control when the carrier fluid is a dispersion of SiO_2 nanoparticles.

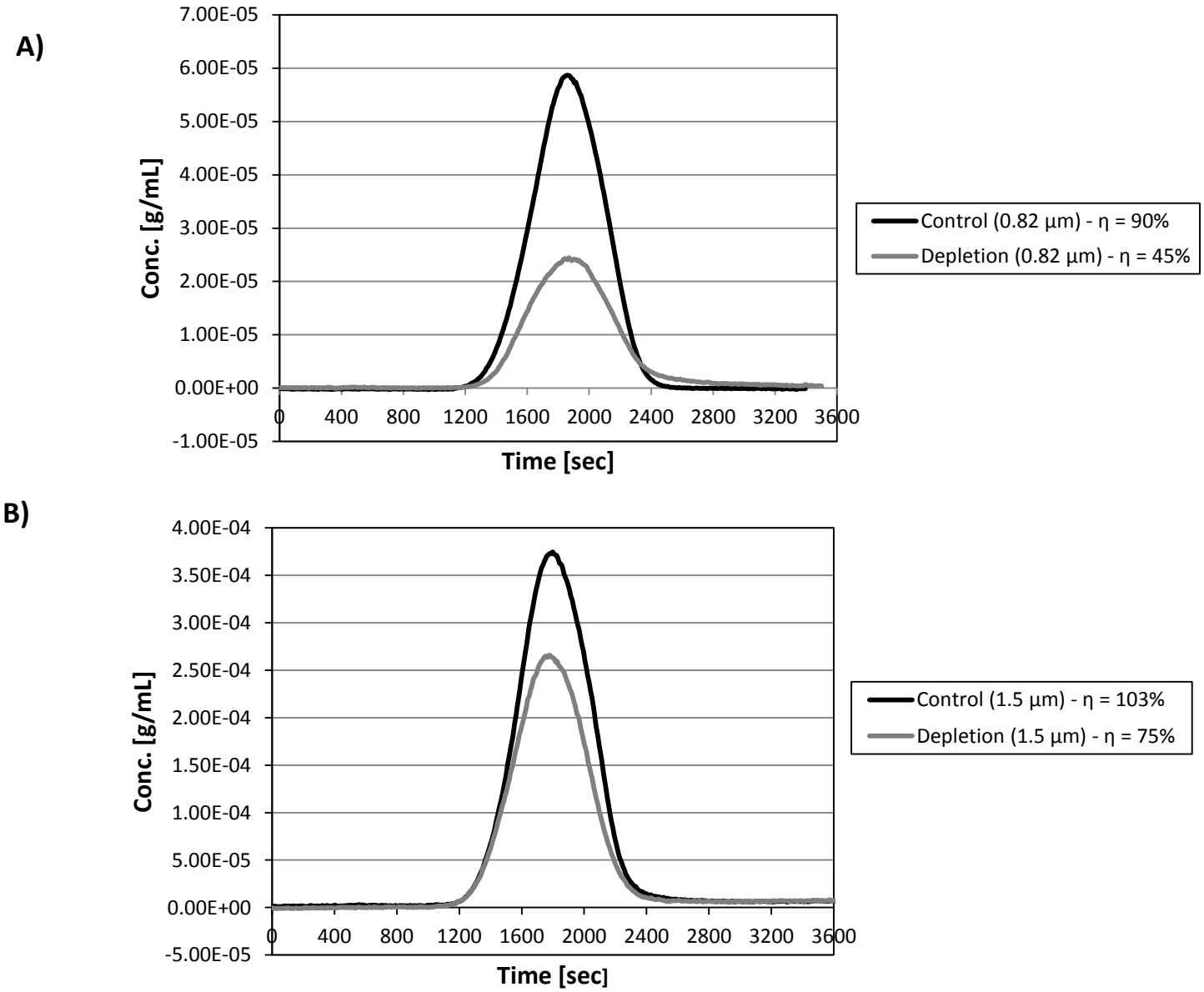

Figure 7: Eluent profiles for the single particle studies. A) Eluent profile for a 0.82 µm particle type for the control, e.g. no nanoparticles, (black line) and depletion (gray line) experiments. B) Eluent profile for a 1.5 µm particle type for the control (black line) and depletion (gray line) experiments.

Reversibility (subsequent release of the PS particles from the column) was not studied in detail, however, some experiments did qualitatively show signs that trapped particle are being released. When the carrier fluid was changed from nanoparticles to deionized water at a higher velocity, two observations were made. First, the top of the column (the 5mm overhead) became slightly turbid

indicating that some particles are being released. Second, a spike in the breakthrough curves was visible even after shifting the baseline intensity. However, because of both the effects of scattering and the increase in velocity it was difficult to see a clear peak in the breakthrough curves. Future experiments will be done at a velocity equal to that of the transport expert, however correcting for the effects of nanoparticle scattering will pose a challenge.

4.2. Binary particle mixture breakthrough curves

Particle mixture studies were done using an experimentally determined equal number density mixture of 0.82 µm and 1.5 µm polystyrene sulfate (PS) particles (2.47 * 10^8 particle/mL for each particle size). When using the manufacturer-provided volume fractions for calculating and making an equal number density mixture, Coulter counter measurements indicated that the mixture was closer to 2:1 small-to-big particles. The cause of this discrepancy is not known. However, for all of the particle mixtures used in the separation experiments the number density was verified using a Coulter counter as being close to 1:1.

For the particle mixture studies, two different trials done on separate days are presented. The pH, conductivities, flow rates, bed length, and nanoparticle concentration are summarized in Tables 1 and 2.

Trial 1		
	Control	**Depletion**
pH	9.5(pulse) – 9.8 (carrier fluid)	9.23 (pulse) -10.3 (carrier fluid)
Conductivity [mS/cm]	1.1 – 1.3	0.99 – 1.1
Salt [mM]	9 to 10	9 to 10
SiO_2 % by vol	0	3
Flow rate [mL/min]	0.3	0.3
Bed length [mm]	375 + 5 (overhead)	375 + 5 (overhead)

Table 1: Summary of parameters for trial 1 of the equal number density PS particle mixture.

Trial 2		
	Control	**Depletion**
pH	10.22 (pulse) -10.47 (carrier fluid)	10.28 (pulse) – 10.44 (carrier fluid)
Conductivity [mS/cm]	0.978 – 1.087	0.982 - 1
Salt [mM]	9 -10	9 – 10
SiO_2 % by vol	0	3
Flow rate [mL/min]	0.3	0.3
Bed length [cm]	375 + 5 (overhead)	375 + 5 (overhead)

Table 2: Summary of parameters for trial 2 of the equal number density PS particle mixture.

As seen in Figure 8, there is a significant difference in the elution profiles between control and depletion experiments. In these plots the concentration could not be calculated from UV/vis measurements because of the combined scattering effects of the binary dispersion of particles. The t = 0 point for all plots shown is at the time the pulse was injected into the column. Eluent samples were collected continuously for 400 seconds in 400 second intervals starting at t = 0. Hence, the breakthrough curves are divided into multiple 400 second regions where Region 1 is defined as $0 < t \leq 400$ sec, Region 2 as $400 < t \leq 800$, and so on. Collected samples for regions 3 thru 8 (from 800 to 3200 seconds) were then analyzed in the Coulter counter and the particle concentration determined. Before being analyzed in the Coulter counter, the collected samples were well mixed and diluted 201 times as described in the Material and Methods section.

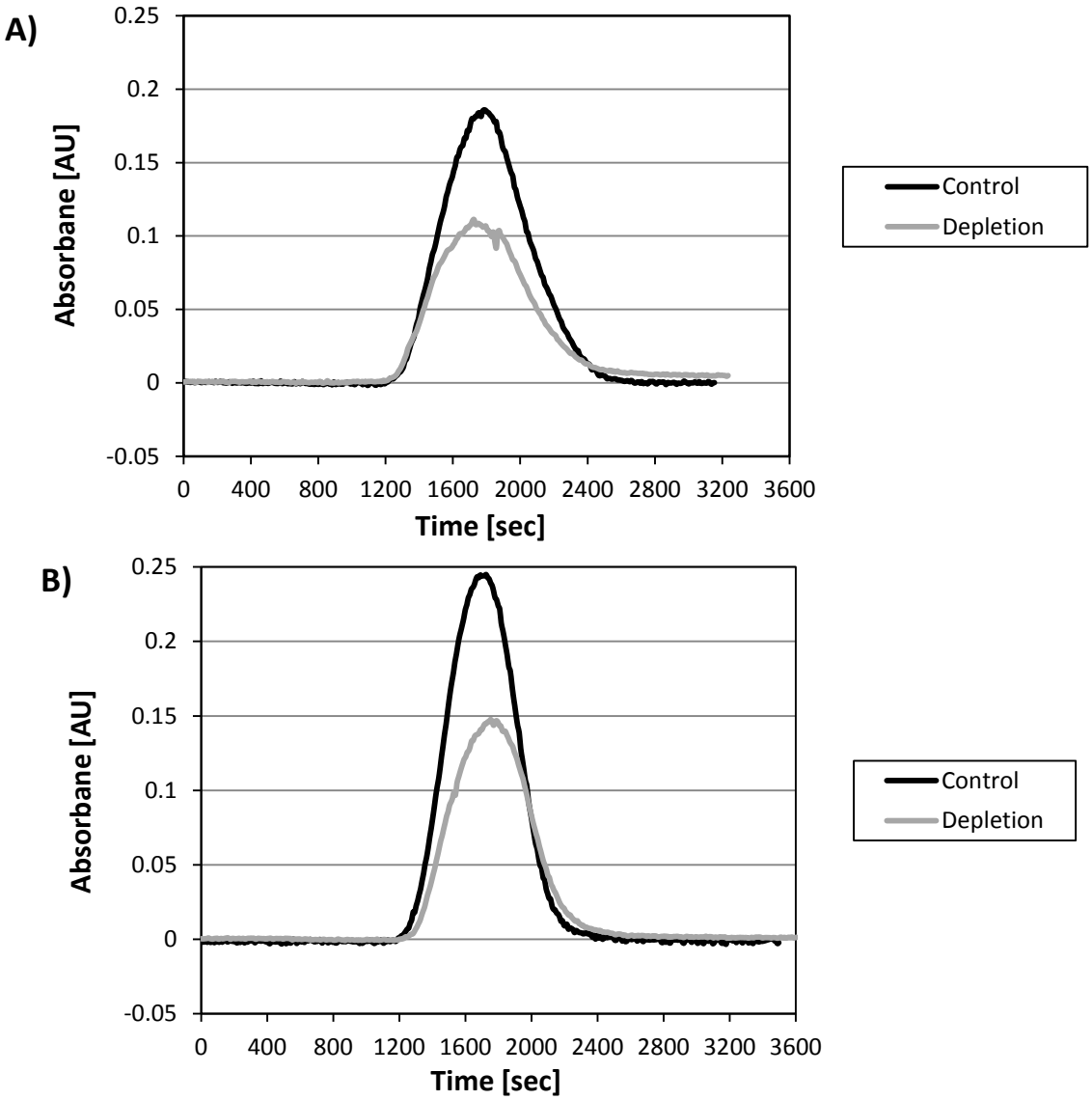

Figure 8: Column elution profiles for an equal density 0.82 µm and 1.5 µm PS particle mixture. Graphs A and B present results from two different trials done on separate days.

4.3 Coulter Counter measurements: Binary Mixture – Control Experiments

As seen in Figure 9A, there is good agreement between the particle number densities and the colloid elution profiles of the control experiments in Figure 8. For example, region C5 should have the highest concentration of particles as it also has the highest absorbance. Figure 9B shows that in the control experiments the ratio of the particles leaving the column is approximately 1:1 for most cases.

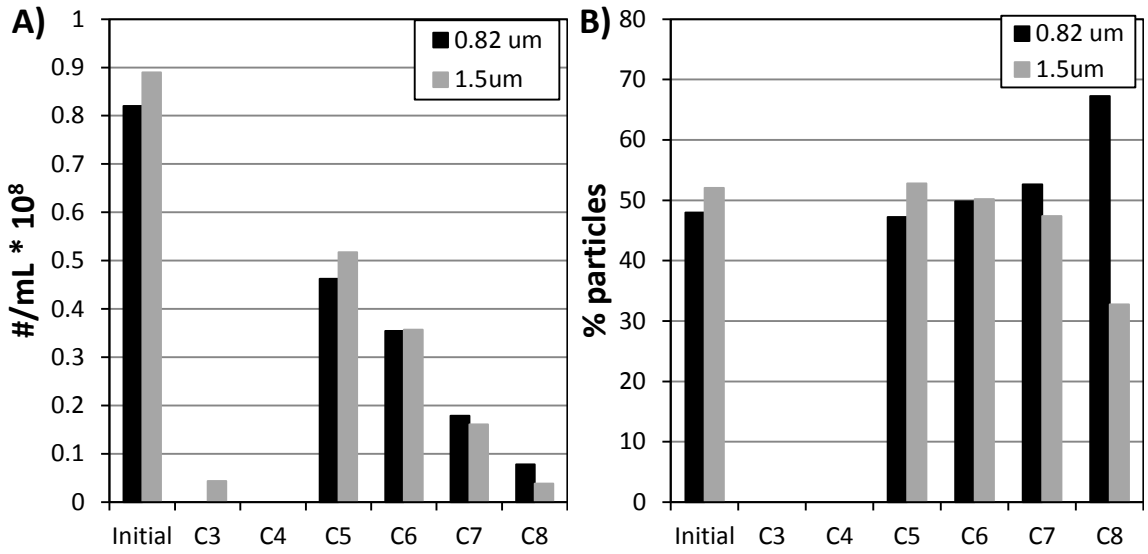

Figure 9: Coulter counter results for the control experiments of Trial 1. A) Particle density vs collected regions for Trial 1 of the control experiments as in Figure 8A. The 0.82 µm PS particles are represented by the black bars and the 1.5 µm PS particles by the gray bars. The 'Initial' data point refers to samples collected prior to injection in the column. The second figure (B) is a plot of the ratio of the percentage of particles in each specific region. For certain regions (C3, C4) the number of particles collected was too low to measure the number density.

As seen in Figure 10 the data from Trial 2 of the control experiments (no nanoparticles) shows very

similar trends to that of Trial 1.

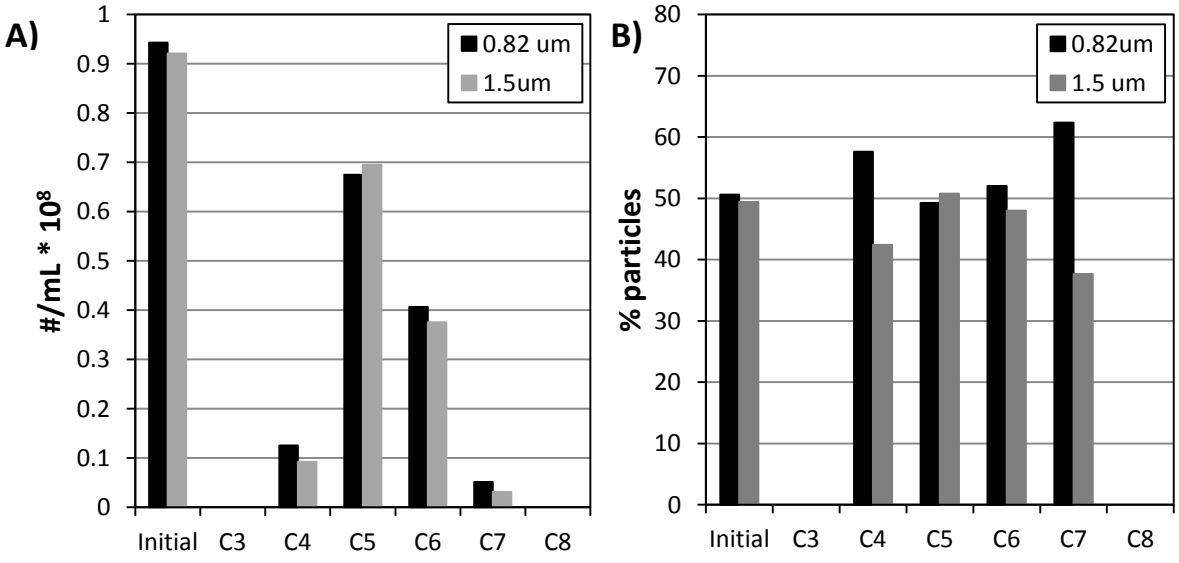

Figure 10: Coulter counter results for the control experiments of Trial 2. A) Particle density vs collected regions for Trial 2 of the control experiments in Figure 8B. The 0.82 µm PS particles are represented by the black bars and the 1.5 µm PS particles by the gray bars. The second figure (B) a plot of the ratio of the percentage of particles in each specific region. For certain regions (C3, C8) the number of particles

collected was too low to measure the number density.

4.4 Coulter counter measurements: Binary mixture – Depletion Experiments

As seen in Figure 11 and 12 there is good agreement between the number densities and the colloid elution profile of the depletion experiments in Figure 8 (Trial 1 and 2). There is however a significant change in the percentages of 0.82 µm and 1.5 µm PS in regions D5 and D6. These results show that there is a change in the capture of the different sized particles experienced within the column, most likely due to the depletion attraction. It is also shown that the larger particles are leaving the column first. The number density results also agree with the recoveries of the single particle studies, where a higher percentage of the smaller 0.82 µm particles remain trapped within the column.

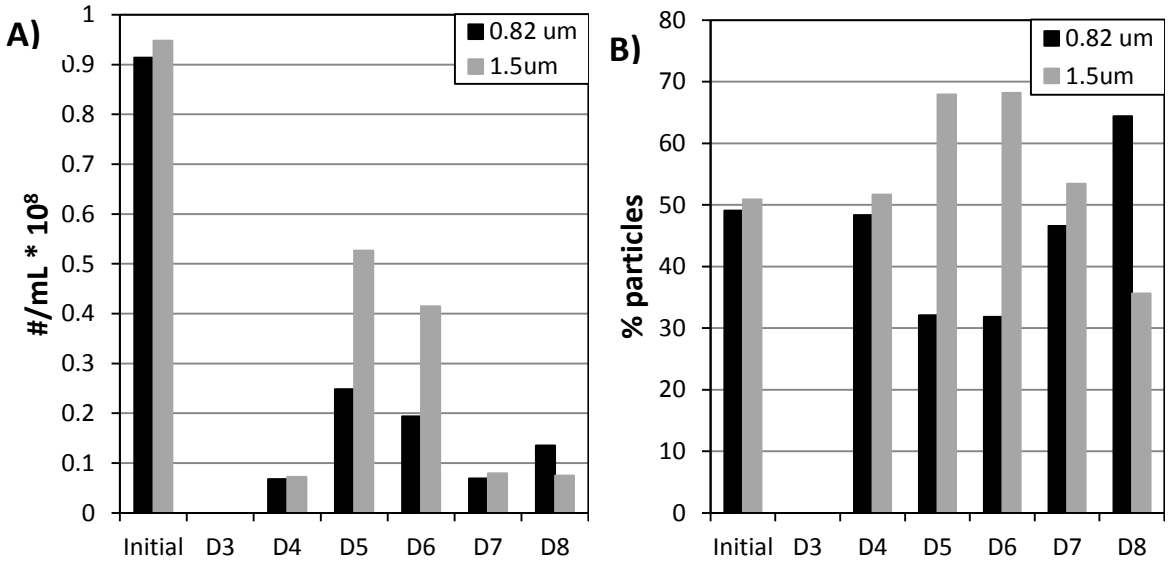

Figure 11: Coulter counter results for the depletion experiments of Trial 1. A) Particle density vs collected region for Trial 1 of the depletion experiment in Figure 8A. The 0.82 µm PS particles are represented by the black bars and the 1.5 µm PS particles by the gray bars. The second figure (B) is plot of the ratio of the percentage of particles in each specific region. As seen, the larger particles have a significantly higher percentage (more than 2:1) in samples D5 and D6. For region D3 the number of particles collected was too low to measure the number density.

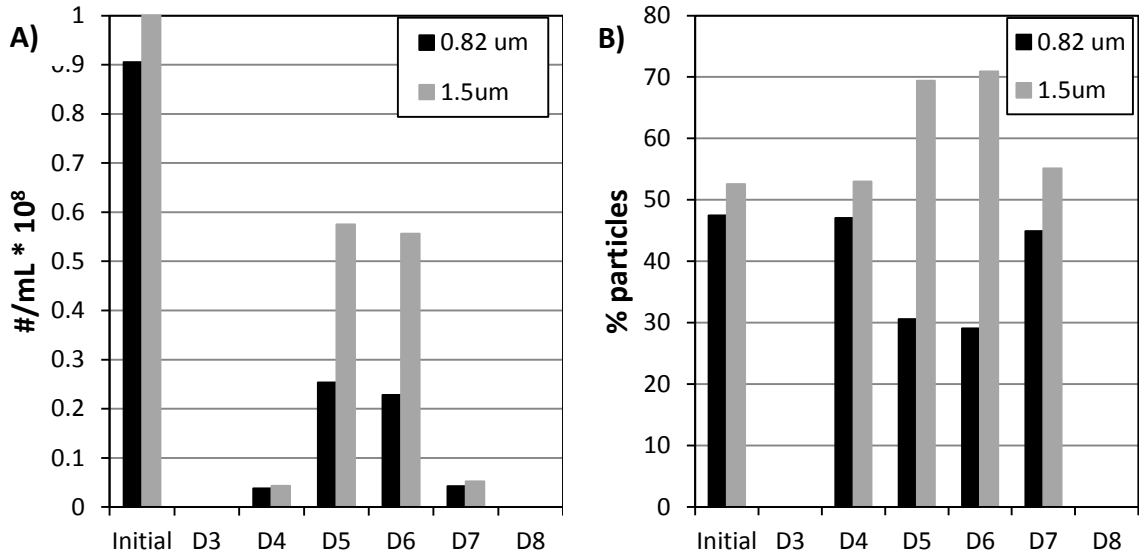

Figure 12: Coulter counter results for the depletion experiments of Trial 2. A) Particle density vs collected region for Trial 2 of the depletion experiments in Figure 8B. The 0.82 µm PS particles are represented by the black bars and the 1.5 µm PS particles by the gray bars. The second figure (B) is a plot of the percentage of particles in each specific region. For regions D3 and D8 the number of particles collected was too low to measure the number density.

4.5 Flow Properties of packed bed

As described in the theory section (2.1) the Reynold and Peclet number can be calculated with knowledge of the bed properties. Using the capillary tube model and an estimate of the porosity the Reynold and Peclet numbers were calculated. A summary of all of the calculated parameters can be seen in Table 4.

Parameters	Empty Column	Packed bed using Capillary Tube Model
ε	1	0.36
l_0 or r_{cap}[cm]	1	0.265
A [cm^2]	3.14	0.221
v or v_{inter} [cm/sec]	0.00159	0.0226
ρ_{water} [g/cm^3]	1	1
µ [g/(cm-s)]	0.001002	0.001002
Re	1.59	12.0
Pe for 0.82um	30,000	226,000
Pe for 1.5 um	55,000	413,000

Table 3: Summary of parameters used for Reynolds and Peclet number calculations.

According to the calculations the flow within the column can be considered laminar, implying that the capillary tube model can be safely applied. Furthermore, because of the magnitude of the Peclet number, the effects of bulk diffusion can be ignored, simplifying the analysis of the particles within the column. However, diffusion will still be important near the capillary walls where the fluid velocity approaches zero. It is in this region where colloidal forces are important.

5. Discussion

5.1 Summary of Results

The single particle studies show that there is a significant change in the particle recoveries when the carrier fluid is a dispersion of silica nanoparticles. In the control experiments, 90% of the 0.82 µm polystyrene particles are recovered and 103% (assumed to be complete recovery) of the 1.5 µm polystyrene particles recovered. The amount of particles that remain in the column can be calculated as 100 – η, where η is the recovery. By comparison, in the depletion experiments, 45% of the 0.82 µm polystyrene particles and 75% of the 1.5 µm polystyrene particles are recovered. The breakthrough curves for both the single particle and binary particle experiments showed a significant tailing effect at starting at times > 2200 seconds. This tail is seen in all of the depletion experiments and can is also seen in the control experiment for the 1.5 µm particle.

The breakthrough curves clearly show that the amount of particles recovered decreases when the carrier fluid was a dispersion of silica nanoparticles. Coulter counter measurements are used to measure the number densities and provided a quantitative analysis of the observed breakthrough curves. The initial binary mixture used for all of the experiments (control and depletion) was a 50/50 mixture of 0.82 µm and 1.5 µm particles. The number density vs collected regions show that in the control experiments the percentage of 0.82 µm and 1.5 µm remains approximately equal throughout the entire breakthrough curve. In the depletion experiments the number density vs collected regions show that there is a significant change in the percentage of polystyrene particles compared to the initial dispersion. The change is best seen in the vicinity of the peak (regions D5 and D6) where the 1.5 µm particles outnumber the 0.82 µm particles by slightly over factor of two. Two different trials of the binary dispersion experiments were done on different days and the results consistent throughout both trials.

5.2 Explanation of Column of results

The breakthrough curves obtained in the control experiments (no nanoparticles) shown in Figure 7 are similar to those of Weronski et al., suggesting that the column is behaving as intended [6]. Since the pH and conductivity for the control and depletion studies are similar, meaning that the electrostatic and van der Waals forces are approximately the same, it is safe to assume that the change in recovery is due to the addition of nanoparticles. The addition of nanoparticles creates a depletion attraction between the polystyrene microparticles and the silica collector beads. Real changes in the packing structure within the packed bed between can be neglected since each set of control and depletion experiments were done on the same day and right after another as described in the material and methods section.

The colloid breakthrough curves in Figure 8 for the binary particle studies also show that there are significant differences between the control and depletion experiments. In this case the breakthrough curves do not provide quantitative information about the degree of separation because of the combined particle scattering effects.

The number density data for the control studies, Figs. 8 and 10, of the binary dispersion show that the particles are leaving the column at almost the same rate, whereas the depletion data, Figs. 11 and 12, show that more of the smaller 0.82 µm particles remain trapped in the column. This result agrees with the single particle studies where much more of the 0.82 µm particles remain trapped in the column compared with the 1.5 µm particles. Hence, the single particle studies can be used to predict the behavior of the binary dispersion.

To further explain the results, potential energy profiles (Fig. 13) for a particle and a plate were calculated using the depletion force model described in section 2.2. In Figure 13A the maximum of the primary repulsive barrier can be considered infinite as the energy goes over 1000 kT at distance less

than 15 nm. In Figure 13B the secondary energy minimum approaches -85 kT and -180 kT for the 0.82µm-plate and 1.5µm-plate cases respectively.

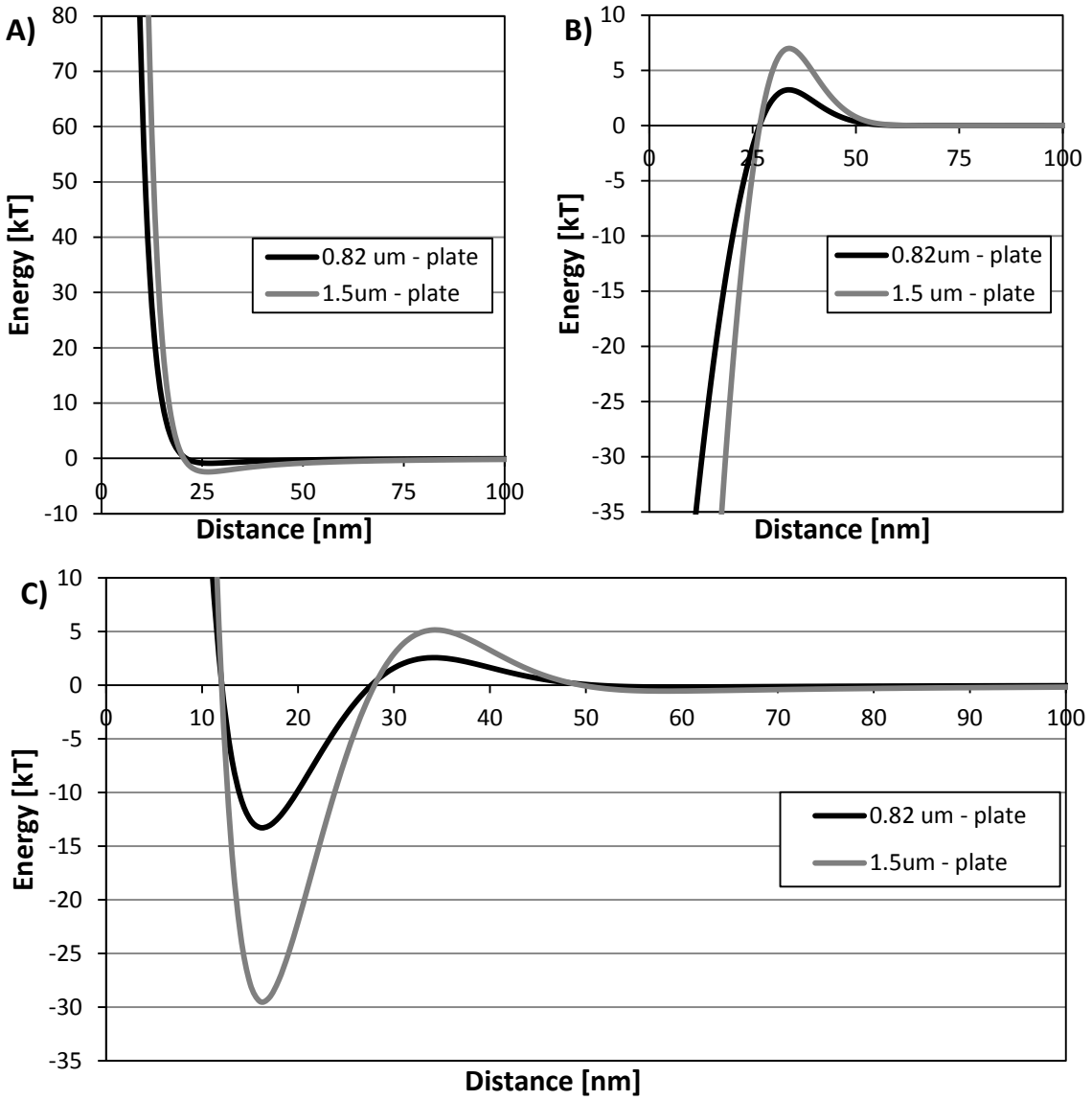

Figure 13: Equilibrium potential energy profiles between a polystyrene particles and a flat silica plate. A) Plot of van der Waals and electrostatic energy, B) plot of the depletion energy, and C) plot of the total energy (sum of van der Waals, electrostatic and depletion energy).

A summary of all of the parameters used for the potential energy profile calculations found in Table 4.

The zeta potential values for polystyrene and silica as a function of pH were picked from the data of Ji et al [23]. For polystyrene and silica the zeta potential was approximately -60 mV at a pH of 10.

Parameter	Value
pH	10
zeta potential – PS [mV]	-60
zeta potential - SiO2 [mV]	-60
Salt [mM]	10
% v SiO2	3
Hamaker Const.: SiO_2-SiO_2 [J]	7.6E-21
Retardation wavelength: SiO_2-SiO_2 [nm]	85
Hamaker Const.: SiO_2-PS [J]	9.9E-21
Retardation wavelength: SiO_2-PS [nm]	105
Hamaker Const.: PS-PS [J]	1.36E-20
Retardation wavelength: PS-PS [nm]	130

Table 4: Parameters for depletion model calculations.

The total energy profile, Fig. 13C, clearly shows that at 3.0% v SiO_2 the 1.5 µm PS particles have to overcome a secondary repulsive barrier of 5 kT, twice the amount the 0.82 µm PS particles, before getting trapped in the secondary energy well at a distance of about 15 nm from the collector surface. Due to the magnitude of the repulsive barrier, the larger 1.5 µm PS particles may not have enough energy to overcome it and more of the particles will tend to leave to column compared to the smaller 0.82 µm particles.

It should be mentioned that since the total energy profiles in Fig. 13C are only calculated up to a second viral coefficient were oscillatory effects are not seen. Oscillatory effects are due to the nanoparticles arranging within the gap between two microparticles and have been studied by Tulpar et. al. Such oscillatory effects gives rise to multiple energy wells measured at distances up to 200 nm [24]. Hence, the particles can potentially remain trapped at distances much larger than 15 nm from the surface.

It should also be mentioned that the predicted energy profiles in Fig. 13 are also for a system at equilibrium. The studied system is dynamic and the hydrodynamic resistance the particles experience when approaching the collector surface must be considered. As the particles approach the collector surface there is a hydrodynamic resistance due to the forced drainage of fluid between the narrowing

particle-collector gap [25]. Due to the competing effects of these forces all of the particles are in a constant state of detachment and attachment and are likely translating across the surface of the collector[6]. This makes calculating the exact trajectory of a particle near the surface of a collector an extremely challenging and interesting problem to be figured out at a later date.

In an effort to develop a more quantitative explanation, the stability ratio W was used. The stability ratio is defined as the ratio of the rate of aggregation in the absence of colloidal interactions to the aggregation rate when there is repulsion between particles. It gives a measure as to how likely a collision between two particles will result in aggregation. The higher the stability ratio the less likely two particles are to aggregate. Our system can be considered as two dissimilar sized spherical particles (polystyrene particle and silica collector bead) where the stability ratio for a particle is roughly approximated as

$$W \approx \frac{1}{\kappa(r_p+r_c)} e^{\frac{\phi_{max}}{kT}} \tag{5.2.1}$$

where κ is the Debye-Huckle parameter, r_p is the radius of a particle, r_c is the radius of the collector, and ϕ_{max} is the magnitude of the repulsive energy barrier [19]. Because of the much larger size of the collector particle, we can approximate the ratio of the stability ratios for the two different particle sizes as

$$\frac{W_{1.5\ \mu m}}{W_{0.82\ \mu m}} = e^{\frac{\phi_{max}^{1.5}-\phi_{max}^{0.82}}{kT}} \tag{5.2.2}$$

where $\phi_{max}^{1.5}(= 5kT)$ is the height of the repulsive barrier for the 1.5 µm particles at 35 nm and $\phi_{max}^{0.82}(= 2.5kT)$ is the height of the repulsive barrier for the 0.82 µm particles at 35 nm obtained from Figure 6C. Thus, $\frac{W_{1.5\ \mu m}}{W_{0.82\ \mu m}} = 12$ means that the 1.5 µm particles are roughly 12 times less likely to get over the secondary repulsive energy barrier and get captured in the secondary energy well. However, this

does not necessarily mean that there are 12 times less of the 1.5 µm particles captured within the column because this is an equilibrium calculation.

Since both the particles and collector beads are negatively charged, deposition onto the collector surface is unfavorable and retention within the column should be reversible due to the magnitude of the primary repulsive barrier (see Fig. 6A). Some experiments showed signs of reversibility when the background carrier fluid was changed to deionized water and repulsion maximized. However, analyzing the UV/Vis data proved very tricky because of the effects of scattering of the nanoparticles when the carrier fluid was changed. Weronski et al. showed that the trapped particles could be released when the carrier fluid was changed [6]. Reversibility should apply to the studied binary dispersion and will be investigated at a later date.

The last point of discussion is the cause and meaning of the tails seen in the breakthrough curves. One possible explanation is that the tails are an effect due to the surface roughness of the particles. The silica collectors used are 'grinding' beads that are likely to have rough surface with many surface asperities. As an example, let's assume that the surface asperities can be thought of as semispherical bumps protruding with a radius r_{bump} and a distance x_{bump} between them. When a particle approaches a collectors surface it can interact with the bump at a distance r_{bump} from the bulk surface or get trapped in the gap x_{bump}. The smaller 0.82 µm particles are more likely to fit in between bumps than the larger 1.5 µm particles. This might explain why both the control and depletion experiments for the single 1.5 µm particle dispersion both show a tail. The larger particles cannot fit in between the bumps and will tend to leave the column at a slower rate compared to the 0.82 µm particles which can remain trapped. Evidence of this can be seen in Trial 1 of the binary particle experiment. In region D8 of Figure 11 the 0.82 µm particles outnumber the 1.5 µm particles by a factor of 2 to 1. This corresponds to the latter part of the tail in Figure 8A. Hence the tail is predominately made up of the 0.82 µm particles showing

that they are being released from the column at a rate slower than the 1.5 µm particles. Overall it can be concluded that the larger 1.5 µm particles are likely to be further from a collector's surface and hence will not remain trapped.

6. Conclusions

These experiments showed that depletion forces can be used to separate a mixture of colloidal particles in one continuous process. From the particular set of experiments done the following conclusion can be drawn:

1. In the absence of silica nanoparticles the single particle dispersion had recovery values near 100%. When silica nanoparticles were introduced (and hence a depletion attraction to the collector surface) the recovery of the 0.82 µm dropped to 45% and the recovery of the 1.5 µm dropped to 75%.
2. The single sized particle dispersion experiments can be used to predict the behavior of the binary dispersion. In the single particle studies more of the 0.82 µm particles remain trapped within the column compared to the 1.5 µm particles. The same trend occurred in the binary dispersion experiments, where more of the 1.5 µm particles were leaving the column.
3. A 1:1 big to small binary particle dispersion can be separated up to a ratio of 2:1 big to small particles in just one pass through the column. Collected samples can potentially be separated once more by running though the column again.
4. Theoretical equilibrium potential energy profiles can be used as a tool for readily finding optimal conditions for separation. The difference in magnitude of the secondary energy barrier for each particle size is the key parameter for predicting the success of a separation.

7. Future Work

The first step will be to study the effect the silica nanoparticle concentration has on the extent of separation. Can ratios greater than 2:1 of big to small particles be obtained by either increasing or decreasing the silica nanoparticle concentration? The potential energy profiles are going to be key in determining the appropriate experimental conditions. The effect of the flow rate (or bed length) can also be investigated as it determines residence time, and hence the number of collisions between particles and collectors beads, of the particles within the column.

An interesting project would be to separate binary dispersion of equal sized but different surface charge particles. A silica-polystyrene microparticle system will be an excellent candidate as silica exhibits a strong pH dependence of its surface charge[23]. In Figure 14 the potential energy profile between a 1.5 µm PS particle and a SiO_2 plate and between a 1.5 µm SiO_2 particle and a SiO_2 plate at a pH of 2, 10 mM salt, and 3.0% v SiO_2 nanoparticles is shown. Under these conditions the surface potential of polystyrene is -60 mV and the surface potential for silica is close to zero (assumed to be 0 mV for simplicity). As seen in the Figure 14, the PS-SiO_2 shows a long range attraction followed by repulsion at a separation distances near 20 nm, whereas, the SiO_2-SiO_2 interaction is only attractive (under these conditions).

Although in this case the repulsive barrier for the PS-SiO_2 interaction might not be enough to prevent deposition onto the surface of a SiO_2 collector, the potential energy profiles between the two cases behave different enough that a separation should be achievable. One way to magnify the difference between the profiles would be by increasing the nanoparticle concentration since increasing the nanoparticle concentration should increase the magnitude of the PS-SiO_2 repulsive energy barrier. The concept here is to find a condition such that one of the particles is stabilized and the other deposits onto the surface of the collector.

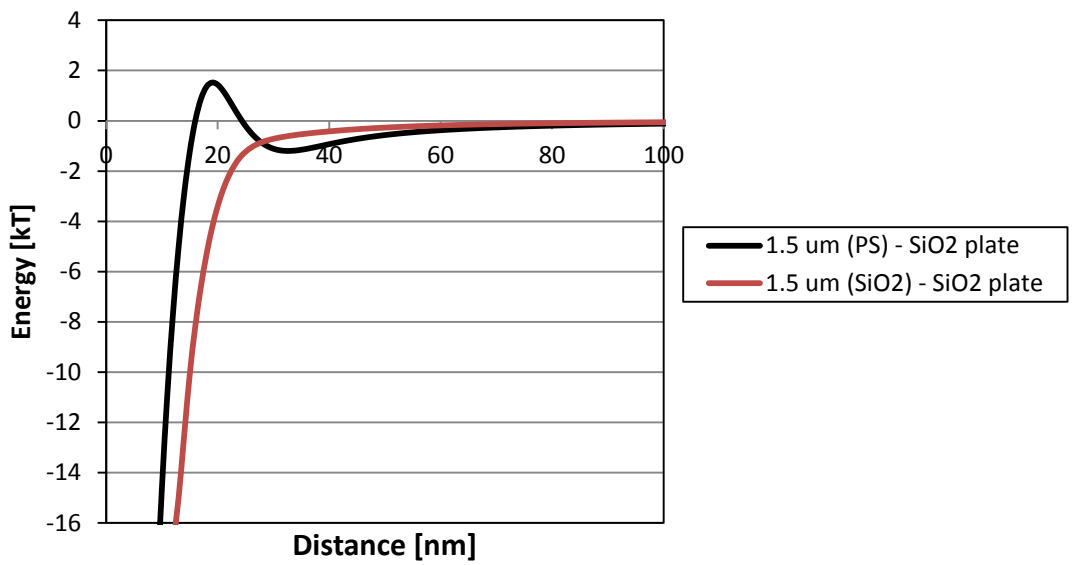

Figure 14: Potential energy profile between a PS particle and a SiO2 plate (black line) and between a SiO2 particle and a SiO2 plate (red line). For both cases the pH is 2, the salt is 10 mM, and the concentration of silica nanoparticles is 3.0% v.

Another interesting project would be to use depletion forces to separate a mixture of single walled carbon nanotubes (SWNT) of different sizes. In this case surfactant micelles are used rather than nanoparticles to achieve the desired separation. Micelles are convenient because the number density (and hence depletion attraction) can be readily increased. In order to model the SWNT the Sharma and Walz depletion model would have to be modified to include non-spherical particle shapes. Potential collaborators include Dr. Ming Zheng, from the Polymers Division of the National Institute of Standards in Technology (NIST), whom has expressed interest in this particular separations project.

References

1. J. Bibette, Depletion Interactions and Fractionated Crystallization for Polydisperse Emulsion Purification. *J. Colloid Interface Sci.* **1991,** *147* (2), 474 - 478.
2. K. Park; H. Koerner; R. A. Vaia, Depletion-Induced Shape and Size Selection of Gold Nanoparticles. *Nano Lett.* **2010,** *10*, 1433-1439.
3. C. Y. Khripin; N. Arnold-Medabalimi; M. Zheng, Molecular-Crowding-Induced Clustering of DNA-Wrapped Carbon Nanotubes for Facile Length Fractionation. *ACS Nano* **2011,** *5* (10), 8258-8266.
4. J. C. Giddings, Field-Flow Fractionation: Analysis of Macromolecular, Colloidal, and Particulate Materials. *Science* **1993,** *260* (5113), 1456-1465.
5. O. N. Katasonova; P. S. Fedotov, Methods for Continuous Flow Fractionation of Microparticles: Outlooks and Fields of Application. *J. Anal. Chem.* **2009,** *64* (3), 228-242.
6. P. Weroński; J. Y. Walz; M. Elimelech, Effect of depletion interactions on transport of colloidal particles in porous media. *J. Colloid Interface Sci.* **2003,** *262* (2), 372-383.
7. S. Asakura; F. Oosawa, On Interaction between Two Bodies Immersed in a Solution of Macromolecules. *J. Chem. Phys.* **1954,** *22*, 1.
8. S. Asakura; F. Oosawa, Interaction between Particles Suspended in Solutions of Macromolecules. *J. Polym. Sci.* **1958,** *33*, 183-192.
9. P. Jenkins; M. Snowden, Depletion flocculation in colloidal dispersions. *Adv. Colloid Interface Sci.* **1996,** *68*, 57-96.
10. R. I. Feigin; D. H. Napper, Stabilization of Colloids by Free Polymer. *J. Colloid Interface Sci.* **1980,** *74* (2), 567-571.
11. R. I. Feigin; D. H. Napper, Depletion Stabilization and Depletion Flocculation. *J. Colloid Interface Sci.* **1980,** *75* (2), 525-541.
12. A. Sharma; J. Y. Walz, Effect of Long Range Interactions on the Depletion Force between Colloidal Particles. *J. Colloid Interface Sci.* **1994,** *168*, 9.
13. C. Tien, *Granular Filtration of Aerosols and Hydrosols*. Butteworths: 1989.
14. J. Bergendahl; D. Grasso, Prediction of colloid detachment in a model porous media: hydrodynamics. *Chem. Eng. Sci.* **2000,** *55*, 9.
15. F. A. L. Dullien, *Porous Media: Fluid Transport and Pore Structure*. Academic Press, Inc.: San Diego, 1992.
16. R. B. Bird; W. E. Stewart; E. N. Lightfoot, *Transport Phenomena*. Second Edition ed.; John Wiles & Sons, Inc.: 2007.
17. P. C. Wankat, *Separation Process Engineering*. Prentice Hall: 2007.
18. P. C. Hiemenz; R. Rajagopalan, *Principles of Colloid and Surface Chemistry*. Third Edition ed.; Macerl Dekker, Inc.: 1997.
19. M. Elimelech; J. Gregory; X. Jia; R. Williams, *Particle Deposition & Aggregation*. Butterworth Heinemann: Oxford, 1995.
20. G. M. Bell; S. Levine; L. N. McCartney, Approximate Methods of Determining the Double-Layer Free Energy of Interaction between Two Charged Colloidal Spheres *J. Colloid Interface Sci.* **1970,** *33* (3), 25.
21. J. Israelachvli, *Intermolecular & Surface Forces*. 2nd Edition ed.; Academic Press: 1992.
22. W. F. K. Y. C. Wu, W. J. Hamer, and Robert L. Kay, Review of Electrolytic Conductance Standards. *J. Solution Chem.* **1987,** *16* (12), 13.
23. S. Ji; D. Herman; J. Y. Walz, Manipulating microparticle interactions using highly charged nanoparticles. *Colloids Surf., A* **2012,** *396*, 51-62.
24. A. Tulpar; P. R. V. Tassel; J. Y. Walz, Structuring of Macroions Confined between Like-Charged Surfaces. *Langmuir* **2006,** *22*, 7.

25. L. A. Spielman, Particle Capture from Low-Speed Laminar Flows. *Ann. Rev. Fluid Mec* **1977,** *9*, 22.